Optics Letters

Cyclic spectra for wavelength-routed optical networks

Bill Corcoran,[1,2,*] Zihan Geng,[1] Valery Rozental,[1] and Arthur J. Lowery[1,2]

[1]Monash Electro-Photonics Laboratory, Department of Electrical and Computer Systems Engineering, Monash University, Melbourne, VIC 3800, Australia
[2]Centre for Ultrahigh-Bandwidth Devices for Optical Systems (CUDOS), Australia
*Corresponding author: bill.corcoran@monash.edu

Received 17 January 2017; revised 16 February 2017; accepted 16 February 2017; posted 17 February 2017 (Doc. ID 284931); published 8 March 2017

We propose occupying the guard bands in closely spaced WDM systems with redundant signal spectral components to increase tolerance to frequency misalignment and channel shaping from multiplexing elements. By cyclically repeating the spectrum of a modulated signal, we show improved tolerance to impairments due to add/drop multiplexing with a commercial wavelength selective switch in systems using 5%–20% guard bands on a 50 GHz DWDM grid.

OCIS codes: (060.1660) Coherent communications; (060.4230) Multiplexing; (060.4265) Networks, wavelength routing.

https://doi.org/10.1364/OL.42.001101

Optical routing of signals using reconfigurable wavelength selective switches in an optical fiber communications network provides redundancy in the case of natural disasters or cable breaks [1], lower cost switching [2], and low energy consumption [3]. Wavelength division multiplexing (WDM) is used to channelize the >4 THz bandwidth available in optical fiber systems employing erbium-doped fiber amplifiers, commonly with channels equally separated by 50 or 100 GHz. The limited resolution of optical filters provided by WDM multiplexers, such as reconfigurable wavelength selective switches [4], leads to the use of reserved spectrum for guard bands between channels, leaving somewhere between 36% and 44% of the available optical spectrum underutilized [5].

Spectral shaping of optical signals provides a method to efficiently use a channel bandwidth. Spectral efficiency can be improved through duo-binary pulse shaping [6], or more complex schemes [7], albeit at the cost of reduced sensitivity. The pulse shaping used to create optical super channels, which have close-to-rectangular signal spectra, can restrict the signal bandwidth to close to the signal symbol rate [8,9], ideally, without a sensitivity penalty. While there are several proposed solutions to allow for signal bands that are spaced very closely (<5% guard band) to be independently routed [10–13], commercially available wavelength selective switch (WSS) devices do not have sufficient wavelength resolution for this task. Intuitively, rectangular optical spectra allow more efficient use of channel bandwidth as defined by optical filtering for WDM multiplexing (mux) and/or demultiplexing (demux) than the sinc-shaped spectra of non-return-to-zero signals that are commonly used in WDM networks. Therefore, spectrally shaped signals are interesting in systems using moderate guard bands (e.g., 5%–33%) to allow for efficient use of installed fiber optic infrastructure.

In Nyquist WDM [8], rectangular spectra are defined for each wavelength through filtering, generally using digital filters before modulating onto an optical carrier. While ideally a Nyquist-shaped signal is inter-symbol-interference (ISI) free, spectral shaping by (for example) an optical filter, can produce impairments resulting in reduced receiver sensitivity [14]. This leaves Nyquist WDM bands vulnerable to impairments from optical add/drop multiplexing in a wavelength-routed system.

Here, we introduce the concept of employing cyclic spectra to provide robustness to optical filtering. The addition of repeated spectral components to a Nyquist-shaped signal provides redundancy that can then be exploited by adaptive equalizers at the receiver side, to reduce the impact of (a) misalignment to the multiplexing filters that define the optical channel and (b) pulse shaping by repeated passes through WDM mux/demux stages.

We show these advantages through experiment in systems employing guard bands of 5%–20%, running 40–47.5 Gbd signals on a 50 GHz grid with add/drop multiplexing emulated using a commercially available liquid-crystal-on-silicon WSS. This demonstration shows that by filling guard bands with redundant data, transmission performance can be improved in wavelength routed optical networks.

Nyquist WDM signals are commonly produced by passing a signal through a root-raised cosine filter at the transmitter at the beginning of an optical link, then matched filtered at the receiver end of the link. This filter is set to have a bandwidth equal to the symbol rate of the signal, restricting the signal to its minimum ISI-free "Nyquist" bandwidth.

In order to generate a spectrally flat signal, the filtered signal should be locally flat (or "white") within the filter bandwidth (as in Fig. 1). This can be achieved by simply interleaving zeros into the signal in the digital (sampled) time domain when the sample rate is greater than 1 Sa/Symb, i.e., by generating a

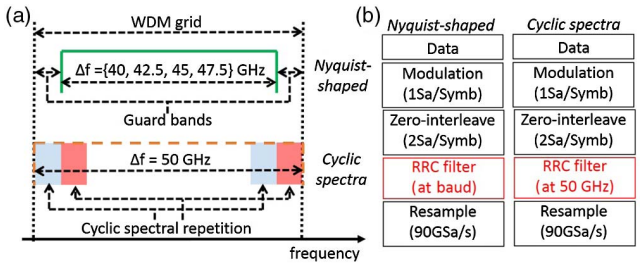

Fig. 1. (a) Description of signal generation through spectral shaping of a zero-interleaved data. With 50 GHz channels, Nyquist-shaped signal spectra occupy a bandwidth equal to their symbol rate, while cyclic spectra signals occupy the full 50 GHz bandwidth with cyclically repeated spectral components. (b) Transmitter DSP flow. Only the filtering block changes from filtering at the symbol rate, to a 50 GHz band.

digital return-to-zero signal. If the sampling rate is an integer multiple of the symbol rate, zero padding in this manner generates a white spectrum across the whole digitally defined band.

If such a signal is shaped with a rectangular filter with the same bandwidth as the signal symbol rate, the signal spectrum contains unique components along its extent. If a filter with a bandwidth greater than the symbol rate is used, there are portions of the spectrum that are repeated at the edges, so that the spectrum is cyclic from one edge to the other. Hence, in this Letter, where we define flat spectra with an excess bandwidth, we denote these signals as having cyclic spectra. This principle is shown in Fig. 1.

The concept of using an excess bandwidth to improve fiber communication system performance has been investigated in several contexts. Using excess bandwidths of over 100%, either through NRZ signaling [15] complex pulse shaping [16] has been shown to improve tolerance to optical nonlinear distortions in transmission. The advantage of having excess signal bandwidth in systems with WSS nodes has been briefly explored in a previous simulation-based investigation [14], where a comparison between 10% and 100% roll-off root raised cosine (RRC) shaping was performed, with the excess bandwidth associated with the 100% roll-off seemingly improving tolerance to filtering impairments. This observation was recently supported by an experimental investigation where bands of a "folded OFDM" signal were more tolerant to add/drop multiplexing when the signal spectrum had redundant components [17]. Moreover, it has been shown that after filtering a cyclic signal spectrum anywhere over its extent, the signal can still be recovered [18], which suggests that signals with cyclic spectra could be tolerant to mux/demux filter-signal frequency misalignment.

Here, signals at line rates of 40–47.5 Gbd, shaped with 1% roll-off RRC filters are compared, with the filter bandwidth set either to the signal symbol rate to provide no excess bandwidth (i.e., forming Nyquist-shaped signals), or to 50 GHz to generate signals with cyclic spectral components (i.e., with excess bandwidths of 5–20%). We choose these values for symbol rates, not to match any required single channel bit rate, but to explore a region of spectral utilization beyond that used in current systems (i.e., with guard bands occupying <36% of the spectrum).

The transmitter and receiver DSP used to generate and receive both Nyquist-shaped and cyclic spectra signals is as follows. The modulated data are interleaved with zeros to provide a 50% duty cycle RZ signal, at 2 Sa/Symb. Note that the RZ signal generated at this point is in the sampled domain and is spectrally white, as opposed to the spectra associated with optically generated RZ signals. QPSK is used as the modulation format. This signal is then filtered by a 1% roll-off RRC filter. In the case of cyclic spectra, the signal is re-sampled to $2 \times 50/BR$ Sa/Symb before RRC filtering (where BR is the signal symbol rate in Gbd), generating a signal with an excess bandwidth of $(50/BR) \times 100\%$ This signal is then re-sampled to match the transmitter digital-to-analog converter rate of 90 GSa/s. No clipping is applied. At the receiver side, the same DSP is used for both the cyclic spectra and the Nyquist-shaped signals, without any modifications. The received waveforms are re-sampled to 2 Sa/Symb, before residual-carrier frequency offset estimation, frequency-domain overlap-add dispersion compensation, pattern synchronization, and dynamic equalization. The dynamic equalizer operates in two stages. First, a training-based least-mean-squares equalizer provides tap weights to initialize a blind constant modulus algorithm equalizer, both with 81 taps. The phase estimation is performed using a training-aided maximum likelihood algorithm before bit-error-rate calculation.

The experimental setup is shown in Fig. 2. Four external cavity lasers (ECLs) are set, spaced by 50 GHz, around a center frequency of 193.075 THz (1552.7 nm). Two pairs of waves separated by 100 GHz are sent to separate complex Mach–Zehnder modulators (CMZMs) driven by a 90 GSa/s (32 GHz electrical bandwidth) arbitrary waveform generator, then recombined to generate a four-channel band with an odd-even channel structure. Polarization multiplexing emulation through delay decorrelation is performed before optical noise loading. The signal can then be passed either directly to the receiver or to a recirculating loop setup consisting of a 80 km span of standard single mode fiber and an add/drop multiplexing emulation node. The node consists of a liquid-crystal-on-silicon WSS, with a 50 GHz bandwidth drop filter defined on a 50 GHz grid. The output of

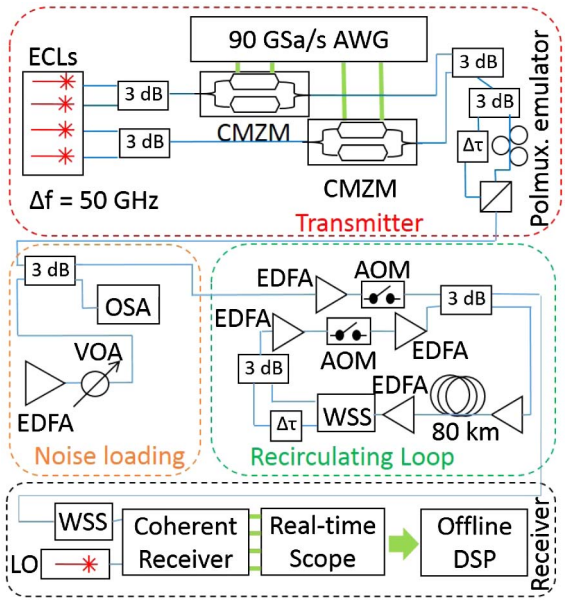

Fig. 2. Experimental setup. $\Delta\tau$, optical delay; OSA, optical spectrum analyzer; AOM, acousto-optic modulator; VOA, variable optical attenuator; LO, local oscillator.

the "drop" port is delay decorrelated from the output of the "express" port, and the two outputs are combined with a 50/50 coupler. This emulates a worst case scenario for optical routing, where each node is set to filter the target channel. The receiver consists of a pre-filter before an integrated coherent receiver with outputs collected and digitized by an 80 GSa/s real-time oscilloscope. Receiver DSP is run off-line.

The Nyquist-shaped and cyclic-spectra signals are first compared in a back-to-back configuration with optical noise loading to ensure that both types of signals are generated with comparable quality. Figure 3 plots the back-to-back performance of both the Nyquist-shaped and cyclic spectra signals, and shows that both types of signals perform similarly against OSNR, indicating that both Nyquist-shaped and cyclic spectra signals are generated with similar quality. This is illustrated by the match in required OSNR for each symbol rate, defined at the 7% ITU G.975.1 hard-decision forward error correction (HD-FEC) threshold ($Q^2 = 8.56$ dB). The degradation in required OSNR scales as expected as the symbol rate is increased.

If these results are interpreted slightly differently, so that performance is plotted against the signal power spectral density over the noise power spectral density [i.e., against S_{sig}/S_{ASE} in Fig. 3(b)], the cyclic spectra have better quality for the same spectral density ratio than the Nyquist-shaped signals, again illustrated by the inset of Fig. 3(b) (which plots the required spectral density ratio against the symbol rate).

In the case of the cyclic spectra, the signal is spread out over more the bandwidth, intuitively resulting in an OSNR penalty counter to the measured result. This is because the dynamic equalizer is able to provide diversity gain to the signal. The diversity in this system comes from the extra redundant spectral components in the cyclic spectrum which, after the dynamic equalizer, effectively result in the coherent addition with the central band to boost performance of the cyclic spectra signal (similar in concept to the spectral diversity scheme used in [19]). This diversity gain (ΔQ) scales as signal bandwidth (Δf) to symbol rate (BR) as $\Delta Q = \Delta f/BR$ [19], explaining why Fig. 3(b) shows "enhanced" performance for the cyclic spectra signal from the diversity gain [see the inset in Fig. 3(b)] scaling as 1, 0.7, 0.5, and 0.2 dB for the 40 to 47.5 Gbd signals, respectively.

In an optically routed link, there can be a significant mismatch (or detuning) between the centers of the passbands of the add/drop multiplexers in the system and the frequencies of the optical signals. When passing through an optical filter or add/drop multiplexing stage, we expect that the main penalty on the filtered channel from this mismatch will be due to channel shaping [14]. As such, we detune the laser frequency of one of the central channels in the four-channel band off its nominal grid value of 193.1 THz and pass the band though a single add/drop node.

Figure 4 shows that detuning affects the Nyquist-shaped signals much more than the signals with cyclic spectra. This is most striking in the 40 Gbd case, where the initial Q^2 penalty due to filtering at 0 GHz detuning is negligible, but grows to 3.7 dB at +5 GHz detuning. A similar trend is seen for the 42.5 and 45 Gbd signals, albeit with significant initial filtering penalties due to channel shaping after a single pass.

At 1 GHz detuning, a Q^2 performance advantage of 0.2, 1.2, 2.4, and 0.7 dB is observed for the 40-, 42.5-, 45-, and 47.5 Gbd signals, respectively. At 5 GHz detuning, this

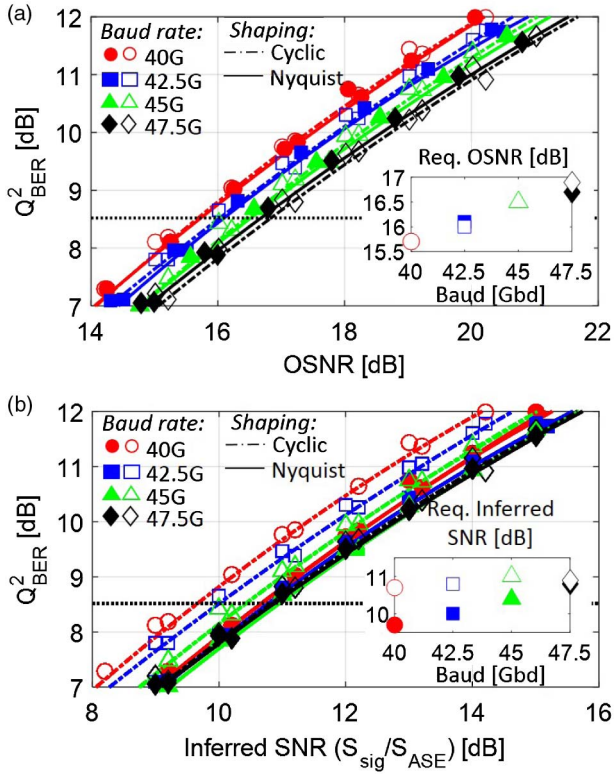

Fig. 3. Back-to-back performance of Nyquist-shaped (solid lines, close symbols) and cyclic spectra (dashed lines, open symbols) signals against (a) OSNR and (b) signal-to-noise power spectral density. Insets: required OSNR or spectral density ratio for each signal tested.

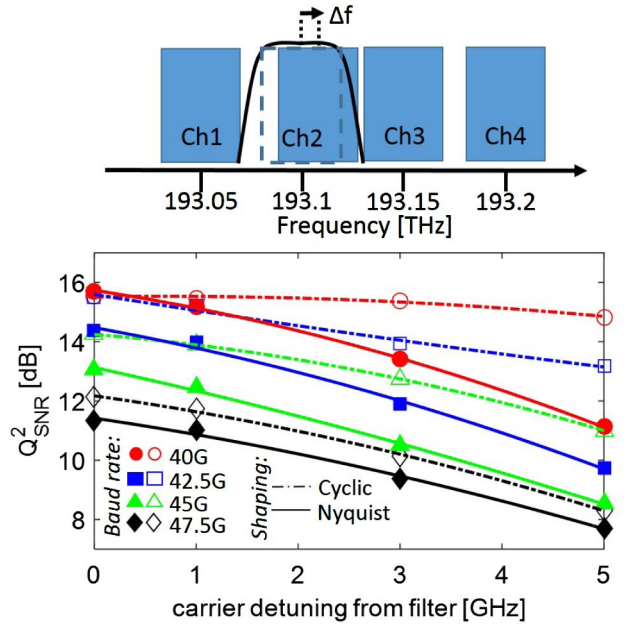

Fig. 4. Performance in the presence of signal frequency detuning off the set 50 GHz grid, after a single 80 km span and add/drop node. The add/drop node is set to add/drop mux a single channel at 193.1 THz, as illustrated by the top inset. Nyquist-shaped, solid lines and closed symbols; cyclic spectra, dashed lines and closed symbols. Inset: an illustration of detuning experiment.

advantage changes to 3.7, 3.4, 2.5, and 0.6 dB for the 40-, 42.5-, 45-, and 47.5 Gbd signals, respectively. For higher symbol rates, there are less redundant data at the edges of the signal spectrum. As such, there is less bandwidth to accommodate loss of signal spectrum due to signal/filter frequency detuning. This indicates that by filling a guard band between channels with redundant data, it is possible to generate signals that are more robust to filter misalignment.

Even when the signal is well aligned to the center of an add/drop filter passband, over multiple add/drop nodes, channel shaping from multiple filters can degrade performance. To ascertain the performance of Nyquist-shaped and cyclic spectra signals through multiple add/drop nodes in a WDM link, both signals were passed multiple times through the emulated add/drop node in the recirculating loop. Either all channels are passed express [Fig. 5(a)], or a single channel is centered at 193.1 THz is dropped and re-added, while the other channels are passed express [Fig. 5(b)], in the same way as for Fig. 4. Here, the add/drop channel is tuned to the nominal center of the filter band. For the "all-pass" configuration, both Nyquist-shaped and cyclic spectra signals have similar performance for each of the signal symbol rates tested. This is consistent with the back-to-back results presented in Fig. 3(a). With the add drop filter in place, we start to see penalties from channel shaping by the add/drop filter. In this case, the cyclic spectra outperform the Nyquist-shaped signals by 1–2 dB in quality factor (Q^2), or allowing an extra node to be reached (i.e., performance above the 7% HD-FEC threshold) for each of the signal symbol rates tested. This indicates that not only are the cyclic spectra signals tolerant to channel misalignment, but also more tolerant than Nyquist-shaped signals to channel shaping over multiple add/drop filter passes (e.g., through multiple ROADM nodes).

We leave some open issues. Here, we have compared Nyquist-shaped to cyclic spectrum signals generated with sharp roll-off RRC filters. One could explore other pulse shapes (e.g., return-to-zero, lower roll-off RRC). Other issues such as channel shaping from node-dependent ROADM-grid detuning and multi-channel add-drop configurations deserve consideration.

In summary, we have demonstrated that signals with cyclic spectra, carrying redundant data in bandwidth normally reserved for guard bands, can improve tolerance to filter misalignment and channel shaping that can occur when using wavelength switching in WDM networks. The technique requires no additional receiver side digital signal processing steps, relying only on adaptive equalization to provide matched filtering. Moreover, the generation of cyclic spectra signals require minor modifications to the digital signal processing at the transmitter side. This technique suggests that it is advantageous to occupy all of the available channel bandwidth in WDM networks, rather than the current approach where signals that slowly attenuate toward the edge of the channel bands.

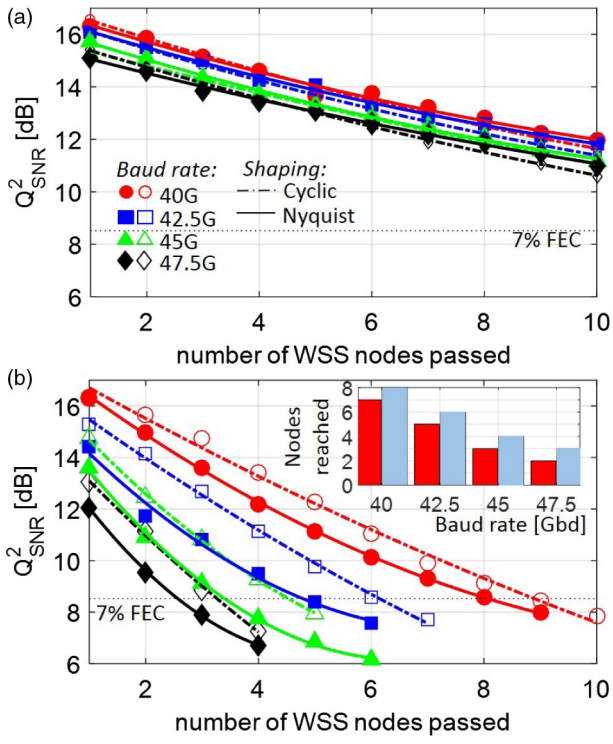

Fig. 5. Multi-pass performance of Nyquist-shaped and cyclic spectra signals through an emulated add/drop multiplexing node with the node set to (a) "all-pass" and (b) add/drop a single channel centered at 193.1 THz. Inset: a comparison of the number of nodes reached by each signal tested.

Funding. Australian Research Council (ARC) (CE110001018, FL130100041).

REFERENCES

1. S. Gringeri, B. Basch, V. Shukla, R. Egorov, and T. J. Xia, IEEE Commun. Mag. **48**, 40 (2010).
2. I. Kaminow, T. Li, and A. Willner, in *Optical Fiber Telecommunications IVB* (Elsevier, 2013).
3. R. S. Tucker, IEEE J. Sel. Top. Quantum Electron. **17**, 261 (2011).
4. C. Pulikkaseril, L. A. Stewart, M. A. F. Roelens, G. W. Baxter, S. Poole, and S. Frisken, Opt. Express **19**, 8458 (2011).
5. J. D. Reis, V. Shukla, D. R. Stauffer, and K. Gass, "Technology options for 400g implementation," http://www.oiforum.com/wp-content/uploads/OIF-Tech-Options-400G-01.0.pdf.
6. J. Li, E. Tipsuwannakul, T. Eriksson, M. Karlsson, and P. A. Andrekson, J. Lightwave Technol. **30**, 1664 (2012).
7. M. Secondini, T. Foggi, F. Fresi, G. Meloni, F. Cavaliere, G. Colavolpe, E. Forestieri, L. Potí, R. Sabella, and G. Prati, J. Lightwave Technol. **33**, 3558 (2015).
8. G. Bosco, V. Curri, A. Carena, P. Poggiolini, and F. Forghieri, J. Lightwave Technol. **29**, 53 (2011).
9. W. Shieh and C. Athaudage, Electron. Lett. **42**, 1 (2006).
10. R. Rudnick, A. Tolmachev, D. Sinefeld, O. Golani, S. Ben-Ezra, M. Nazarathy, and D. M. Marom, in *European Conference on Optical Communication (ECOC)* (IEEE, 2014), p. 1.
11. S. J. Fabbri, S. Sygletos, A. Perentos, E. Pincemin, K. Sugden, and A. D. Ellis, J. Lightwave Technol. **33**, 1351 (2015).
12. W. Wei, L. Yi, Y. Jaouën, M. Morvan, and W. Hu, Opt. Express **23**, 19010 (2015).
13. B. Corcoran, C. Zhu, J. Schröder, L. Zhuang, B. Foo, M. Burla, W. P. Beeker, A. Leinse, C. G. H. Roeloffzen, and A. J. Lowery, J. Lightwave Technol. **34**, 1824 (2016).
14. M. Filer and S. Tibuleac, in *IEEE Photonics Conference* (IEEE, 2014), p. 268.
15. C. Behrens, S. Makovejs, R. I. Killey, S. J. Savory, M. Chen, and P. Bayvel, Opt. Express **19**, 12879 (2011).
16. B. Châtelain, C. Laperle, K. Roberts, M. Chagnon, X. Xu, A. Borowiec, F. Gagnon, and D. V. Plant, Opt. Express **20**, 8397 (2012).
17. B. Corcoran, C. Zhu, B. Song, and A. J. Lowery, Opt. Express **24**, 29670 (2016).
18. A. J. Lowery, J. Schröder, and L. B. Du, Opt. Express **22**, 1045 (2014).
19. V. Ataie, D. Esman, B. P.-P. Kuo, N. Alic, and S. Radic, Science **350**, 1343 (2015).